POLITECNICO DI TORINO
Repository ISTITUZIONALE

# Gallium based hollow silica nanospheres for the acid-catalyzed upgrading of glycerol: Enhanced activity disclosed via an in-depth nuclear magnetic resonance approach

*Original*
Gallium based hollow silica nanospheres for the acid-catalyzed upgrading of glycerol: Enhanced activity disclosed via an in-depth nuclear magnetic resonance approach / Soumoy, L., Morena, A., Armandi, M., Fiorilli, S., Fusaro, L., Debecker, D.P., Aprile, C.. - In: JOURNAL OF CATALYSIS. - ISSN 0021-9517. - 447:(2025). [10.1016/j.jcat.2025.116143]

*Availability:*
This version is available at: 11583/3008406 since: 2026-06-15T12:36:59Z

*Publisher:*
Academic Press Inc.

*Published*
DOI:10.1016/j.jcat.2025.116143

*Terms of use:*

This article is made available under terms and conditions as specified in the corresponding bibliographic description in the repository

*Publisher copyright*
Elsevier preprint/submitted version

Preprint (submitted version) of an article published in JOURNAL OF CATALYSIS © 2025, http://doi.org/10.1016/j.jcat.2025.116143

(Article begins on next page)

18 November 2026

**Gallium based hollow silica nanospheres for the acid-catalyzed up-grading of glycerol: enhanced activity disclosed via an in-depth nuclear magnetic resonance approach.**

*Loraine Soumoy [a]‡, Anthony Morena [a]‡, Marco Armandi [b], Sonia Fiorilli [b], Luca Fusaro [a*], Damien P. Debecker [c], Carmela Aprile [a*]*

*[a] Unit of Nanomaterials Chemistry, Department of Chemistry, NISM, University of Namur,5000 Namur, Belgium*

*[b] Department of Applied Science and Technology, Politecnico di Torino, 10129 Torino, Italy*

*[c]Université catholique de Louvain (UCLouvain), Institute of Condensed Matter and Nanosciences (IMCN), 1348 Louvain-la-Neuve, Belgium*

‡: These authors contributed equally to this work

Key words: Hollow silica-based nanospheres, glycerol conversion, Trimethylphosphine, Heterogeneous catalysts, Solid State NMR, solid acids

## ABSTRACT

Ga-doped hollow silica nanosphere and nanotubes were synthetized using a soft template sol-gel method. The low dimensional morphologies (0D or 1D) were obtained by simply adjusting the stirring speed during the synthesis procedure. The two materials were fully characterized using different techniques such as ssNMR, $N_2$ physisorption, XRD, TEM or ICP-OES. The influence of the calcination temperature on the coordination environment of gallium as well as the accessibility of the gallium active sites was proved via $^{71}$Ga ssNMR. The acid features of the solids were studied via a combined approach based on FT-IR of adsorbed ammonia and $^{31}$P ssNMR using trimethylphosphine as a probe molecule. The latter technique allows unveiling a higher Brønsted/Lewis acid sites ratio of Ga-nanospheres as compared to Ga-nanotubes, probably as a consequence of the more defective spherical shell. Both nanostructures were tested for the conversion of glycerol to solketal. Ga-nanospheres revealed improved catalytic performance in comparison with the corresponding nanotubes and displayed outstanding activity with respect to other solid catalysts reported in the literature and tested under the same reaction conditions. Moreover, they proved to be stable and reusable in multiple cycles. The E-factor calculated under the best condition was below 1 thus proving the sustainability of the process.

## 1. INTRODUCTION

Over the past decades, the synthesis of porous silica-based materials with low dimensionalities (particles diameter < 100 nm), tunable particle size, porosity and architectures was widely explored.[1, 2] The interesting properties of low dimensional solids are mostly related to their

nanoscopic dimensions, hence to their high surface area-to-volume ratio, spatial confinement, and high surface curvature making them suitable for different applications, including catalysis and biomass valorization.[3, 4] Generally, these structures are synthetized either *via* soft or hard templating approach. In particular, the soft templated sol-gel strategy involves the formation of a "soft" organic scaffold followed by the hydrolysis of a silica precursor which condenses around the pre-formed organic structure, generating a well-defined silica network.[5, 6] Recently, among all the possible silica-based materials obtained using a 'soft' templating strategy, the controlled synthesis of hollow silica nanotubes and nanospheres has been highlighted.[7] In-depth studies of their formation mechanism, allowed identifying the parameters enabling the selective design of one of the two nanostructures. In particular, the amount of swelling agent (toluene) stabilized by the F127 surfactants proved to be the key parameter controlling the change in morphology.[7] One of the most alluring feature of silica nanostructures is the isomorphic substitution of a controlled fraction of Si atom by a selected heteroelement (≠Si), generally a metal cation (M) to design materials with additional tailored functionalities.[8] This substitution is favored by the flexibility of the silica framework, which compensates the generated structural strains by slight modifications of bond lengths and angles.[9] In the case of zeolites, it is reported that this isomorphic substitution is possible between atoms characterized by similar sizes (critical difference about the radii of c.a. 15%) and electronegativity (critical difference of electronegativity values about c.a. 0.4 a.u.).[10-12] One of the most interesting consequences of the isomorphic substitution of Si atoms by M is the enhanced acidity of the resulting solid, due to the generation of Brønsted (B) and Lewis (L) acid sites. The B/L ratio is influenced by multiple parameters among which the most relevant is represented by the nature of the metal cation. When M is a trivalent cation such as $B^{3+}$, $Al^{3+}$or $Ga^{3+}$ the creation of B active sites is favored. The insertion of tetravalent cations, such as $Ti^{4+}$, $Sn^{4+}$ or $Hf^{4+}$, can also lead to the formation of acid sites with a preferential formation of L acidity. Indeed, once M is bonded to three (trivalent element) or four (tetravalent) oxygen atoms, the oxygen electron pair of a nearby surface silanol group can interact with the empty orbital of the M atom. Electron density is withdrawn from the oxygen atom of the hydroxyl group, enhancing the overall acidity of the hydroxyl proton which act as source of Brønsted acidity (Figure 1b or 1d). The generation of Lewis acid sites is also possible when surface -OH groups are not interacting with the M atom. In this situation, the empty orbital of the M element can interact with the electron pair of a Lewis base (Figure 1a or 1c).[13, 14] Although these considerations are very formal, they have the merit of clearly explaining the presence of both Brønsted and Lewis acid sites in M-doped silica frameworks. In many cases, complex situations including intricated combination of Brønsted and Lewis acid sites are also encountered.[9, 13, 14]

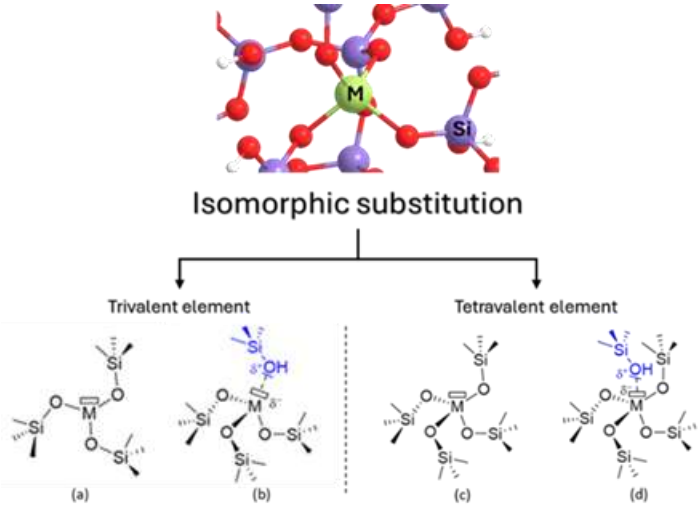



**Figure 1** Insertion of a heteroelement (M) in the silica framework. The insertion of a trivalent M leads to the generation of a Lewis (a) or a Brønsted (b) acid site. The insertion of a tetravalent M can also lead to the generation of a Lewis (c) or Brønsted (d) acid site. The rectangle represents an empty orbital of the heteroelement (M).

For these functionalized silicates, in the perspective of their applications, the precise description of the metal environment and the acidity properties is a crucial endeavor. Over the past years, different techniques coupled with the adsorption of basic probe molecules were employed to unveil the nature of acidic active sites in metallosilicates. In particular, the overall acidity was studied *via* the use of probe molecules (e.g. pyridine and ammonia) in combination with temperature programmed desorption (TPD) or coupled to infrared spectroscopy (FT-IR).[15] Moreover, in the last three decades it emerged that detailed acid features such as nature, concentration, and strength of acid sites can be investigated *via* solid-state nuclear magnetic resonance (ssNMR) selecting a suitable probe molecule containing NMR-sensitive nuclei such as $^{13}C$, $^{15}N$, or $^{31}P$. Among all the possible probe molecules, trimethylposphine (TMP) could be employed in this field.[16] The use of this molecule is quite advantageous due to the wide chemical shift range of $^{31}P$ NMR, allowing the easy identification of the different acid sites, but also thanks to the high sensitivity of the $^{31}P$ dipolar nucleus and 100% natural abundance.[17, 18] Acid mesoporous metallosilicates have been employed as heterogeneous catalysts in various sustainable chemical processes, such as the synthesis of alkyl lactates and other valuable chemicals from glycerol and its derivatives.[19, 20] Glycerol, a major by-product of biodiesel production, can be valorized through a large panel of reactions[21] including the acetalization with acetone to produce solketal.[15, 22-24] Solketal has applications as green solvent,[25] in pharmaceuticals formulation,[25] and as a fuel additive,[26, 27] supporting circular economy principles.[23] This reaction aligns with various green chemistry principles since it uses a

renewable feedstock, and displays a high atom economy (88% if full selectivity is considered) together with a potentially low E-factor.[28, 29] Moreover, it can be performed with acetone playing both the role of solvent and reactant hence limiting the use of other more toxic co-solvents, at relatively low reaction temperature, and in continuous flow mode.[30, 31] Both homogeneous[26, 32] (e.g., $H_2SO_4$, HCl) and heterogeneous[33-36] (e.g. zeolites, metal-organic frameworks, M-silicates) catalysts were already reported, with Brønsted acid sites generally showing higher efficiency than Lewis acid sites in converting the acetone-glycerol adduct to solketal.[37] Focusing on mesoporous silica materials, Li et al. reported that the activity of a series of mesoporous silicate such as Sn-MCM-41 is higher than an ultra-stable zeolite such as Al-TUD-1.[38] The authors attributed this improvement to a combination of features such as the enhanced accessibility of the active sites, improved diffusion properties and favorable environment of the catalytically active species.[38] Indeed, the morphology of a catalyst can have a direct influence on different parameters affecting its activity such as the specific surface area, the accessibility of the active sites or the mass transport of reactants and products. Moreover, in a previous work based on Hf-doped silica nanotubes, the authors highlighted how the nature of active site as well as the physicochemical characteristics of the support were both crucial to enhance the conversion of glycerol into solketal.[15] Among all the trivalent metal, the insertion of gallium in mesoporous silicates showed promising results for the targeted reaction.[24, 39-43] It is generally accepted that the highest B/L ratio showed the better catalytic activity. However, a clear relationship between acid properties and morphology has not yet been well defined. Considering the importance of the B/L ratio in the reaction under investigation, a more detailed study of the strength of the active sites should be also carried out.

Herein, a micelle templated sol-gel approach to design two low-dimensional silica-based nanostructures was considered. Novel hollow nanospheres and nanotubes embedding gallium as single site in the silica framework were efficiently synthesized. The tetrahedral insertion of gallium was probed via solid state $^{71}$Ga nuclear magnetic resonance. The latter technique also allows evidencing a clear dependence of the thermal treatment and exsolution phenomenon of gallium which was correlated with the catalytic properties. The acidity features were investigated with two different techniques: $^{31}$P ssNMR and FT-IR using TMP and ammonia as probe molecules, respectively. Importantly, TMP assisted $^{31}$P ssNMR allowed unveiling the different nature of Brønsted and Lewis sites providing relevant insights on the influence of the morphology on the catalytic activity. It deserves to be mentioned that TMP assisted $^{31}$P ssNMR is a poorly explored technique due to the easily oxidable nature of the probe employed. Herein a carefully designed experimental set-up was proposed to achieve highly reproducible results while preserving the nature of TMP. An in-depth

ssNMR investigation was also performed employing acetone as probe molecule to provide further insights on the availability of the Ga active sites. Both nanotubes and hollow nanospheres were tested for the conversion of glycerol to solketal. The latter solid displays better performance compared to nanotubes and outstanding activity with respect to other catalysts previously reported. Furthermore, Ga-doped silica nanospheres were reused in multiple cycles thus providing the stability of the material under selected reaction conditions.

## 2. Materials and Methods

### *2.1 Synthesis of silica hollow nanospheres (Si-NS)*

The syntheses were performed in a 250 mL covered glass container maintained at a temperature of 12°C with a magnetic stirring of 550 rpm. As reported in a previous work the stirring speed is a key parameter to determine the final morphology of the solid.[7] The glass container was 70 mm in diameter and 133 mm in height and the stirring bar was 6 mm in diameter and 30 mm in length. 1.0 g (0.080 mmol) of Pluronic F127 was added to 60.0 mL of HCl 2 M. The mixture was stirred for one hour to ensure the complete solubilization of the templating agent. Then, a mixture of tetraethyl orthosilicate (TEOS − 2.8 g – 13 mmol) and toluene (3.0 mL − 0.028 mmol) was prepared. This solution was added dropwise to the templating agent solution. After 24 h, the pH was adjusted to the final value of 9, using 10,5 mL of an aqueous ammonia solution (30 %). The reaction mixture was then stirred for another 24h at 12°C. After filtration of the reaction mixture and washing with 500 mL of distilled water, the obtained gel was lyophilized overnight. The collected white powder was finally calcined under air at 550°C for 5 h with a heating rate of 2 °C/min. The sample was denoted Si-NS.

### *2.2 Synthesis of silica Nanotubes (Si-NT)*

The syntheses were performed in a 250 mL covered glass container maintained at a temperature of 12°C with a magnetic stirring of 250 rpm for nanospheres. As reported in a previous work the stirring speed is a key parameter to determine the final morphology of the solid.[7] The glass container was 70 mm in diameter and 133 mm in height and the stirring bar was 6 mm in diameter and 30 mm in length. 1.0 g (0.080 mmol) of Pluronic F127 was added to 60.0 mL of HCl 2 M. The mixture was stirred for one hour to ensure the complete solubilization of the templating agent. Then, a mixture of tetraethyl orthosilicate (TEOS − 2.8 g – 13 mmol) and toluene (3.0 mL − 0.028 mmol) was prepared. This solution was added dropwise to the templating agent solution. After 24 h, the pH was adjusted to the final value of 9, using 10.5 mL of an aqueous ammonia solution (30 %). The reaction mixture was then stirred for another 24h at 12°C. After filtration of the reaction mixture and washing with 500 mL of distilled water, the obtained gel was lyophilized overnight. The collected white powder

was finally calcined under air at 550°C for 5 h with a heating rate of 2 °C/min. The sample was denoted Si-NT.

### *2.3 Synthesis of Ga-doped silica hollow nanospheres*

The preparation of Ga-doped silica hollow nanospheres closely follows the procedure outlined in paragraph 2.1. After stirring for 2 hours following the addition of the TEOS and toluene solution, a solution of $Ga(acac)_3$ dissolved in 1 mL of 2 M HCl (Si/Ga molar ratio of 74) was added dropwise to the reaction mixture under continuous stirring. The subsequent steps remain unchanged from those described in paragraph 2.1. The resulting sample was denoted Ga-NS.

### *2.4 Synthesis of Ga-doped silica nanotubes*

The preparation of Ga-doped silica nanotubes closely follows the procedure outlined in paragraph 2.2. After stirring for 2 hours following the addition of the TEOS and toluene solution, a solution of $Ga(acac)_3$ dissolved in 1 mL of 2 M HCl (Si/Ga molar ratio of 74) was gradually added dropwise to the reaction mixture under continuous stirring. The subsequent steps remain unchanged from those described in paragraph 2.2. The resulting sample was denoted Ga-NT.

### **2.5** *Characterization*

Transmission electron microscopy (TEM) images were taken using a Philips Tecnai 10 microscope operating at 80 kV. Prior to imaging, the impregnated solids were dispersed in ethanol *via* ultrasonication and deposited on a copper grid.

Nitrogen adsorption-desorption analyses were carried out at 77 K with a volumetric adsorption analyzer (Micromeritics ASAP 2420). Prior to the analysis, the samples were pre-treated 16 hours at 170 °C under reduced pressure (0.1 mbar). The Brunauer–Emmet–Teller (BET) method was applied in the 0.05-0.20 relative pressure ($P/P_0$, $P_0$ = 101.3 kPa) range to calculate the specific surface area, the total pore volume was determined from the amount of adsorbed $N_2$ at a relative pressure of 0.99 and the pore size distributions were calculated from the adsorption branch of the isotherm using the Barrett–Joyner–Halenda (BJH) method with the Kruk-Jaroniec-Sayari (KJS) correction. The micropore volume was calculated via the t-plot method, applied to the adsorption branch of the isotherms in the thickness range of 3.5–5.0 Å, using macroporous silica as reference.

Chemical combustion analysis or elemental analysis (CHN or EA) analysis were performed in a Flash 1112series EA ThermoFischer – Interscience with a GC-TCD detector. CHNS analysis operates in two steps: 1. An oxidation-reduction reactor (containing Cu) is placed in a furnace at 950°C under a continuous helium flow. The precisely weighed sample is introduced into the reactor, followed by a

brief injection of oxygen to initiate the oxidation or reduction reaction, depending on the sample. This process generates various gases: carbon produces $CO_2$, hydrogen forms $H_2O$, nitrogen generates $N_2$, and sulfur produces $SO_2$. These gases are then separated in a gas chromatography (GC) column, and their concentrations are determined based on their intensity and a calibration curve. Using the precisely measured sample mass, the concentration values allow us to calculate the percentage of each element in the sample.

Thermogravimetric analysis was performed under air flow from 25 to 900 °C with a heating rate of 10 °C/min in a Mettler Toledo TGA STAR system.

$^{1}$H-NMR liquid-state spectra were recorded at room temperature on a JEOL ECX 400 MHz spectrometer, operating at 9.4 T and equipped with a broadband 5 mm probe.

Solid-state (ss) cross-polarization (CP) and direct excitation (DE) magic angle spinning (MAS) $^{29}$Si nuclear magnetic resonance (NMR) spectra were recorded at room temperature, on a Jeol ECZ-R 600 MHz spectrometer operating at 14.1 T, equipped with an AUTOMAS probe. The samples were packed in 3.2 mm zirconia rotors and spun at 10 kHz. TPPM $^{1}$H decoupling with an RF field of 46.6 KHz was applied during the acquisition time. DE experiments were carried out with a recycle delay of 300 s and a number of scans equal to 800. CP MAS experiments were performed using a contact time of 5 ms, a recycle delay 5 s and a number of scans equal to 12569. $^{29}$Si Chemical shifts were referenced externally to Sodium trimethylsilylpropanesulfonate (DSS) at -0.1 ppm.[44]

Solid-state $^{71}$Ga NMR spectra were recorded on the same spectrometer, using a spinning frequency of 20 kHz. Note that the calcined samples were analyzed immediately after the thermal treatment and in the same conditions as the catalytic tests. Indeed, spectra reported in Fig. 3 were acquired immediately after calcination and the rotors were packed in air. A batch of Ga-NS was synthesized, five different portions were collected, and each portion was treated only at one temperature (corresponding to the one indicated in Figure 3). Concerning the experiment on the dehydrated samples and the one with the addition of TMP or $H_2O$, the sample was pre-treated like the one used for the acidity measurement via $^{31}$P ssNMR (*vide infra*). The spectra were recorded using a Hahn echo sequence and the following acquisition parameters: a relaxation delay of 0.3 s, an excitation pulse of 2 μs (90°) and 1.0 ms acquisition time. Spectra in Fig. 3 were registered with a number of scans between 150000 and 300000. Spectra in Figure S16 were recorded using 300000 scans (corresponding to c.a. 25 h of analysis). The chemical shift scale was calibrated at room temperature with respect to a sample of solid gallium nitrate (0.0 ppm).[45]

Solid-state $^{31}$P MAS NMR spectra were acquired at room temperature on a 400 MHz Varian VNMRS spectrometer equipped with a 4 mm Varian/Chemagnetics T3 probe and operating at 9.4 T (161.9 MHz for $^{31}$P) and a spinning frequency of 8 kHz. Samples were packed in 4 mm Bio solids cavern

rotors provided by Phoenix NMR. They were sealed using a non-vented top spacer in PCTFE equipped with two o-rings. The experimental conditions included a π/2 flip-angle of 3.4 μs, a relaxation delay of 6 s, an acquisition time of 20 ms and a total of 1280 scans. TPPM $^{1}$H decoupling with an RF field of 46.6 KHz was applied during the acquisition time. Chemical shifts were referenced externally to ammonium dihydrogen phosphate ($(NH_4)H_2PO_4$) ($^{31}$P: 0.81 ppm)[16]. A portion of the sample was dehydrated in two stages. Initially, it was calcined at 550 °C for 8 hours. Then, the sample was placed under vacuum ($10^{-3}$ mbar) in a Schlenk line system for 1 hour. The 4 mm rotor was packed with the solid sample in an inert argon atmosphere inside a glovebox, and 5 μL of liquid-phase trimethylphosphine (TMP) was added to the sample inside the rotor. To remove the excess of TMP, the sample was exposed to a vacuum of $10^{-6}$ mbar for 4 hours at 100 °C using a homemade setup similar to that described in the literature.[46]

Inductively coupled plasma optical emission spectroscopy was employed to determine the chemical composition of the materials using an Optima 8000 ICP-OES Spectrometer. Prior to the analysis, the samples were digested in a mixture of *aqua regia* and HF.

FT-IR measurements were performed in transmission mode by using a Bruker Tensor 27 spectrometer equipped with a liquid nitrogen-cooled mercury–cadmium–telluride (MCT) detector, operating at a 2 $cm^{-1}$ resolution. Thermal pre-treatment and probe molecules dosage were carried out using a standard vacuum frame, in an IR cell equipped with KBr windows. The samples were pressed into self-standing wafers and outgassed for 1 h under secondary vacuum (residual P < 0.1 Pa) at 673 K before adsorption/desorption experiments. IR spectra were recorded after dosing $NH_3$ (5.5 purity) on the pre-treated samples, at the maximum equilibrium pressure of 2000 Pa. Subsequently, the equilibrium pressure was progressively decreased and, finally, samples were outgassed under vacuum at beam temperature (*ca.* 30 min *in situ*). Spectra were normalized with respect to the integrated absorption of silica framework overtone bands, since wafers with similar density were used (*ca.* 5 $mg/cm^2$). The spectra are reported as difference spectra obtained by subtracting the IR spectrum of the naked sample (*i.e.* before probe molecule adsorption).

### *2.6 Conversion of glycerol into solketal*

In a 10 mL round-bottom flask, 0.920 g (10.0 mmol) of glycerol, 10 mg of freshly calcined catalyst, and 2.32 g (40.0 mmol) of acetone were added. All the reactants were used as purchased without any further treatment. The mixture was heated at 50 °C under 800 rpm stirring. Typical tests were carried out for two hours. After this time, the mixture was cooled down to room temperature and homogenized *via* the addition of 3 mL of absolute ethanol. The solution was centrifugated to separate the catalyst from the reaction mixture (4500 rpm, 10 min). 500 μL of the supernatant were taken from

the filtrate and the solvent was evaporated under reduced pressure (10 min, 50 mbar). Finally, 600 µL of deuterated DMSO were added for quantitative $^{1}$H NMR experiment. The influence of the external diffusion on the catalytic activity was tested evaluating the yield of solketal at a stirring speed of 800 rpm and 1000 rpm. No change of yield at 2 hours was observed, confirming the absence of external diffusion when a stirring speed of 800 rpm is used.

### *2.7 Hot-filtration experiment*

In a 10 mL round-bottom flask, 0.920 g (10.0 mmol) of glycerol, 10 mg of the freshly calcined catalyst, 0.60 mL of absolute ethanol, and 2.32 g (40.0 mmol) of acetone were added. The mixture was heated at 50 °C under 800 rpm stirring. After one hour of reaction, the solution was transferred in a 15 mL centrifugation tube and centrifuged to separate the catalyst from the reaction mixture (4500 rpm, 10 min). The catalyst was dried and calcined for further analyses. A sample of the supernatant (500 µL) was recovered, dried under reduce pressure (10 min, 50 mbar), and analyzed by $^{1}$H NMR using deuterated DMSO (600 µL) as solvent. The filtrate was stirred and kept at 50 °C for another 5 hours and stirred at 800 rpm. A second $^{1}$H NMR analysis of the reaction mixture was then performed to assess the evolution in solketal yield.

### *2.8 Recycling experiment*

Glycerol (3.22 g, 0.035 mol), acetone (4 equiv.) and the freshly calcined catalyst (70 mg), were added in a round-bottom flask. The mixture was heated at 50 °C under 800 rpm stirring for 1 h. After this time, the mixture was cooled down to room temperature and homogenized *via* the addition of 3 mL of i-PrOH. The catalyst was separated from the mixture by millipore filtration. A sample of the filtrate (500 µL) was recovered, dried under reduce pressure (10 min, 50 mbar), and analyzed by $^{1}$H NMR using deuterated DMSO (600 µL) as solvent. Then, the solid was calcined in air at 550 °C for 5 h (heating rate: 2 °C/min). The subsequent catalytic tests were carried out by repeating this procedure from the beginning (the quantities were adapted as a function of the mass of recovered catalyst).
Despite the several calcinations steps the nominal ratio (Si/M) of 74 was always preserved; this value was confirmed via ICP analysis performed on the catalyst after the last catalyst cycle.

### *2.9 E-factor*

Glycerol (2.76 g, 0.030 mol), acetone (4 equiv.) and the catalyst (Ga-NS, 30 mg), were added in a round-bottom flask. The mixture was heated at 50  C under 800 rpm stirring for 16 h. After this time, the round-bottom flask was connected to a distillation apparatus to recover the excess of acetone.

## 3. RESULTS AND DISCUSSION

**3.1 Synthesis and study of the Physico-chemical properties of Ga-NS.** Ga-doped silica hollow nanospheres (Ga-NS) with Si/Ga molar ratio of 74 were synthesized adapting a previously reported procedure and applying a pH adjusting step.[7, 15] The pH adjusting step (from pH 0 to 9) was implemented to favor the insertion of $Ga^{3+}$ in the silica shell while preserving the nanostructure. The physico-chemical properties of Ga-NS were characterized *via*, *inter alia*, TEM, $^{71}$Ga ss MAS NMR, FT-IR and ssNMR using respectively ammonia and trimethylphosphine (TMP) as a probe molecule. The morphology of Ga-NS was first inspected *via* transmission electron microscopy (Figure 2). The as-synthesized (Figure 2a) and calcined solids (Figure 2 b and c) display very similar structure thus indicating that the thermal treatment needed to efficiently remove the surfactant (*vide infra*) had no detrimental effect on the nanostructure of the NS. The micrographs of Ga-NS revealed the presence of spherical architectures characterized by a hollow interior and a wall thickness of *ca.* 2 nm. Some pores can be noticed in the shell of the nanospheres, indicated by white arrows of Figure S1. The size of these pores is not easily measurable due to their non-circular shape but the larger are in the small mesopore range. From the perspective of catalytic applications, it is inferred that reactants should have access to the inner part of the Ga-NS structure. Note that Ga-NS were produced in triplicate showing high reproducibility even when the synthesis was scaled up.

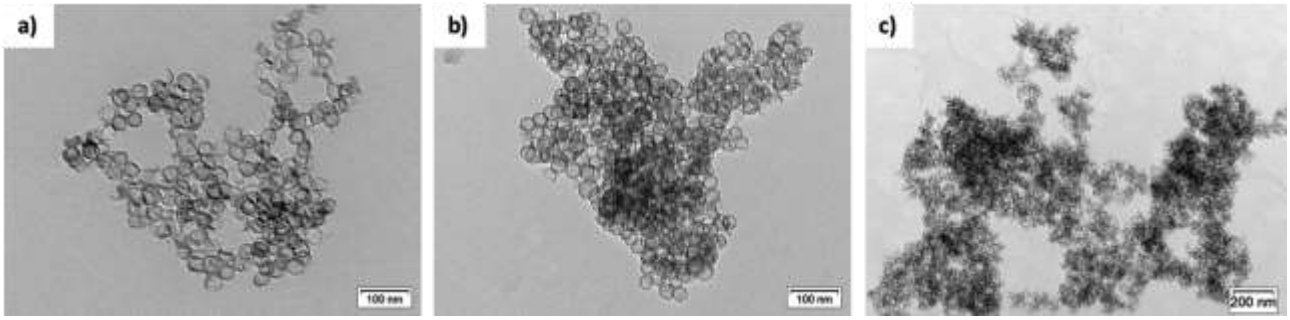



**Figure 2** - TEM micrograph of as-synthesized (a), calcined (b, c) Ga-NS. High-resolution TEM images are available in Figure S1.

The content of gallium within the sample was verified *via* inductively coupled plasma optical emission spectroscopy. The quantity of gallium, expressed in mol of gallium per gram of solid, was equal to 2.1 x $10^{-4}$ mol/g and is hence, in excellent agreement with the nominal value of 2.2 x $10^{-4}$ mol/g (Si/Ga mol = 74). To investigate the insertion of gallium in the silica framework and its coordination environment, ss $^{71}$Ga MAS NMR experiments were

undertaken. Figure 3 shows the presence of two signals centered at around 140 ppm and 0 ppm. The more intense signal (140 ppm) is usually associated to Ga species with a low coordination degree, *i.e.* in a tetrahedral environment in the silica framework while the signal at 0 ppm can be ascribed to the presence of Ga species in octahedral coordination (most probably extra framework oligo- or polymeric $Ga_xO_y$ species).[47-49] Here, gallium is shown to be mainly inserted in the silica framework. Note extra-framework species are expected to be poorly active in the conversion of glycerol to solketal.[41] To gain better insights on the nature of the residual extra-framework gallium species, X-ray diffraction (XRD) in the wide-angle range was conducted as well (Figure S2). The amorphous XRD pattern reveals the absence of large crystallites of gallium oxide thus indicating that the signal at 0 ppm can be attributed to small $Ga_xO_y$ domains. In the perspective of a deeper understanding the origin of these extra-framework species highlighted in Figure 3, $^{71}$Ga MAS NMR experiments were performed on the as-synthesized Ga-NS (before calcination). It is worth mentioning that the solids display a low quantity of Ga, less than the 2 wt%. The low amount together with the fact that the Ga cations are inserted in an amorphous silica environment, can explain the low signal to noise ratio observed for the $^{71}$Ga NMR spectra. Interestingly, the spectrum (Figure S3) displays only one signal centered at 150 ppm, revealing the presence of tetracoordinated gallium species (Ga IV) and confirming that the synthesis protocol allowed the proper insertion of gallium in the silica framework. The thermal treatment used to remove the templating agent (conditions: 550 °C, 5 h, under air) is most probably inducing the formation of the $Ga_xO_y$ species. To shed more light on the origin of this phenomenon, the influence of the calcination temperature ($T_{calc.}$) on the Ga coordination environment (Figure 3) was investigated treating the as synthesized Ga-NS at various temperatures (250 °C to 650 °C). When Ga-NS was thermally treated at 250 °C or 350 °C, an intense signal centered at *ca.* 150 ppm was observed, indicating that the Ga species are still in a tetrahedral environment.[39, 41] When the temperature of the calcination was higher than 350 °C, a second signal centered at around 0 ppm appears indicating the formation of extra-framework gallium species (Ga VI). The octahedral contribution is even clearer in the Ga-NS calcined at 650 °C thus indicating that at this temperature a higher quantity of gallium oxide species are most probably formed at the surface of the solid. The octahedral $Ga_xO_y$ probably arose from the migration of tetrahedral Ga species from the bulk of the silica matrix to the surface (a phenomenon called "exsolution"[50]) with the consequent formation of extra-framework gallium oxide clusters. The increase of $T_{calc}$ also led to the broadening and shift of the more intense contribution from 150 ppm up to 140 ppm. Based on literature data, this behavior could be ascribed to the emergence of surface pentacoordinate Ga species (Ga V).[51] The presence of Ga V further supports the hypothesis on the migration of intraframework Ga IV species to the surface of the silica walls. If catalytically active, the increase in surface of Ga

species constitutes a favorable feature for a heterogeneous catalyst. Furthermore, when comparing the spectra of Ga-NS calcined at 350 °C and at 550 °C (same number of scans), an evident decrease of the signal to noise ratio (S/N) was observed. All the previous findings led us to hypothesize that increasing the calcination temperature resulted in a higher heterogeneity in the chemical environment of the gallium sites. These intraframework Ga sites are expected to be less symmetrical and surrounded by an amorphous chemical environment (*vide infra* for more details).

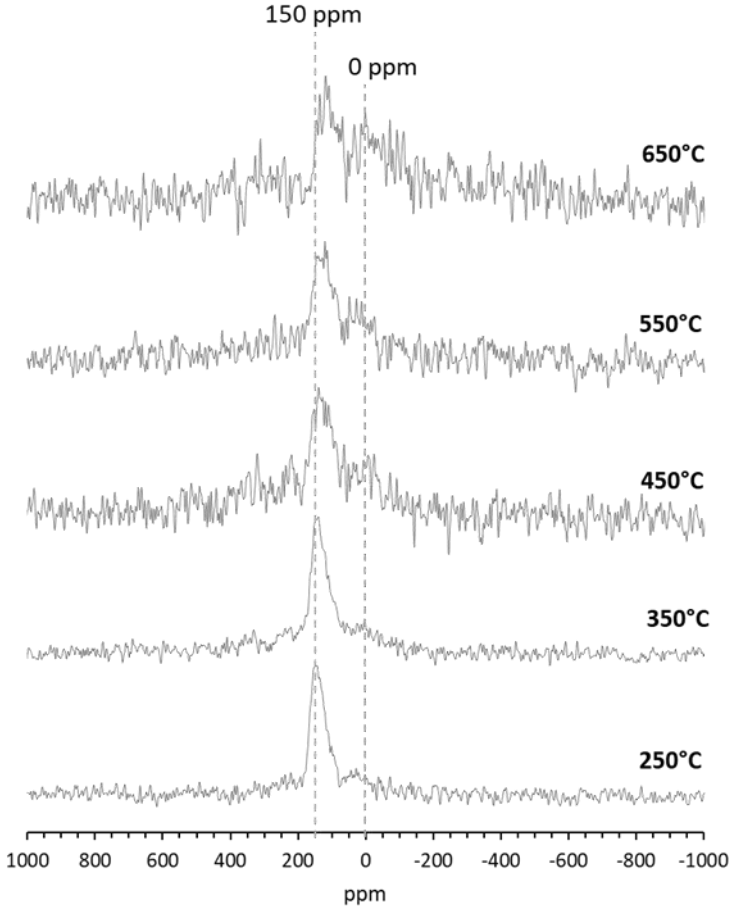



**Figure 3** - ss $^{71}$Ga MAS NMR of Ga-NS calcined at temperature ranging from 250 °C to 650 °C.

It is known that a mild calcination conditions induces only a partial removal of the organic surfactant.[39, 52] To verify if the different thermal treatments allowed removing efficiently the templating agent ($PEO_{100}$-$PPO_{65}$-$PEO_{100}$), the weight % of carbon was evaluated *via* CHN analysis (see table S1). When Ga-NS was calcined at 250 °C, 3.0 wt.% of residual carbon was found in the sample. This amount dropped to 0.9 wt.% when $T_{calc}$ was increased to 350 °C. The solids calcined at 450 °C and 550 °C displayed a percentage of carbon equal to 0.9 and 0.5 wt.%, respectively. The combined information obtained from ss $^{71}$Ga NMR and CHN analysis indicated that starting from 350 °C, an efficient removal of the templating agent (wt.% C < 1 %) was achieved while a progressive

appearance of Ga species in pentahedral (at first) and octahedral (later) environment is observed (figure 3). The former are expected to be highly active surface species while the later are supposed to present none or negligible catalytic activity.[41] To confirm this last statement and investigate the influence of the Ga coordination environment in the conversion of glycerol to solketal, Ga-NS calcined from 350 °C to 650 °C were tested. The solid treated at 250°C was excluded from this comparison due to the high residual carbon content. The catalytic tests were performed at 50 °C, with acetone playing the role of both reactant and solvent. The activity of the solids was evaluated through the yield of solketal obtained after 2 hours of reaction (Figure 4).

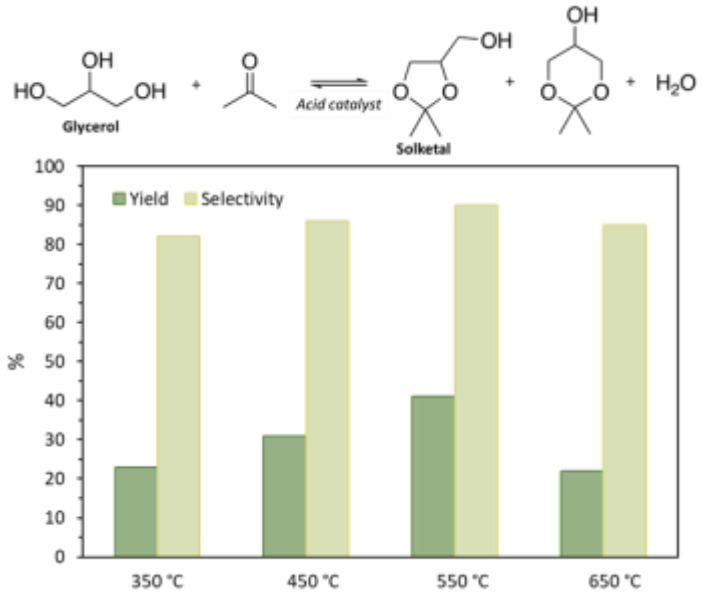



**Figure 4 -** Yield of solketal influenced by the calcination temperature of Ga-NS. Reaction conditions: 50 °C, 2 hours, 10 mg of catalyst, Gly: Ac = 1 (0.01 mol): 4. 2,2-dimethyl-1,3-dioxan-5-ol (6-membered ring) and water are the main by-products of the reaction. Conversion estimated via $^{1}$H NMR of the reaction mixture. A more detailed comparison is presented in Table S1

From the evaluation of the catalytic performances of Ga-NS (Figure 4) a progressive increase of the catalytic activity emerged from Ga-NS calcined at 350 °C to 550 °C, while a drop of catalytic performances was detected for the solid calcined at 650 °C. Regardless of the calcination temperature, Ga-NS is highly selective toward the production of solketal (above 80 %). To verify if the decrease of activity for Ga-NS calcined at 650 °C could be ascribed to a change in the structure of the solid, a TEM analysis was performed. Figure S4 showed that the solid retained its well-defined spherical hollow morphology. Hence, the drop in catalytic performances can be ascribed to the significant amount of extra-framework $Ga_xO_y$ (see figure 3). The rise of activity when $T_{calc}$ was increased from 350 °C to 450 °C can also be explained in terms of Ga coordination environment. The correlation between $^{71}$Ga MAS NMR spectra and catalytic activity led us to hypothesize that Ga IV could not be

the sole species responsible for the efficient production of solketal. Pentahedral Ga species could contribute to facilitate the formation of the desired product, also because Ga V should mostly be located at the surface of the nanospheres shell, hence easily accessible for the reagents. Note that in the case of aluminosilicates, pentacoordinate Al sites were shown to induce both Lewis and Brønsted acidity.[53, 54] A further increase of $T_{calc}$ from 450 °C to 550 °C didn't modify strongly the Ga chemical environment of the solids which display very similar $^{71}$Ga MAS NMR spectra. In this case, the increased activity could be ascribed to different hydrophilic-hydrophobic properties of the catalyst surface.[11, 39, 52, 55] While hydrophilic surfaces can favor glycerol adsorption in proximity of the active sites, hydrophobic surfaces would help the removal of water produced as by-product of the reaction, locally shifting the reaction towards the formation of solketal. To investigate if the difference of catalytic activity could arise from a difference in the hydrophilic-hydrophobic properties of the catalyst surface, Ga-NS calcined at 450 °C and 550 °C were analyzed *via* thermogravimetric analysis (TGA) (see Table S1). In order to evaluate the quantity of physisorbed water, the weight loss of the samples was quantified between 30 °C and 170 °C.[39] The quantity of water lost by the sample calcined at 550 °C (4.4 wt.%) was smaller compared to Ga-NS calcined at 450 °C (6.1 wt.%). This result indicates that an increase of the calcination temperature favors the formation of more hydrophobic surfaces, hence improving the production of solketal. Recently, a similar behavior was observed in the case of aerosol-prepared silicates, tested in the conversion of the targeted reaction.[39] Optimizing the calcination temperature of the heterogeneous catalyst is hence fundamental to enhance its catalytic activity.[39] In the case of Ga-NS, a calcination temperature of 550 °C allowed obtaining a solid in which most of the templating agent was eliminated, the catalyst surface is slightly more hydrophobic, and the environment of the Ga species is favorable for the target reaction.

### 3.2 Ga-NS and Ga-NT comparison and study of their acidic properties using ssNMR and FT-IR.

To push further the understanding of the different parameters influencing the catalytic activity, Ga-doped silica nanotubes were synthesized as well (Ga-NT). This solid was synthesized selecting the optimized protocol (same reaction conditions and calcination at 550°C). The characterization (Figure S5-S8) shows the presence of well-defined nanotubes (Figure S5) and indicates that the two solids, despite showing different morphology (NS and NT), exhibit very similar Ga environment as evidenced by $^{71}$Ga NMR analysis (Figure S12). A more precise quantitative analysis of tetrahedral, pentahedral and octahedral Ga species in both NS and NT is hindered by the broad overlapping contributions. It should be mentioned that the overall Ga

content determined via ICP remained unchanged in both nanotubes and nanospheres after calcination, matching the nominal Si/M ratio of 74.

The textural properties of both Ga-NS and Ga-NT calcined at 550 °C were evaluated through $N_2$ adsorption-desorption analysis (Figure S9). The isotherms of Ga-NT and Ga-NS showed a sharp increase in adsorbed volume at a relative pressure close to 0.01, indicating the existence of micropores in the shell of the silica structure. An abrupt increase of adsorbed volume occurred at a relative pressure of *ca.* 0.9 (*i.e.* capillarity condensation), suggesting that the materials feature large mesopores. This observation agrees with TEM analysis which revealed a large internal cavity of the tubes/spheres (*ca.* 20 nm). The desorption branch of the isotherms, joining the adsorption branch at a relative pressure of *ca.* 0.7 for nanospheres and *ca.* 0.8 for nanotubes, indicates that the access to the nanostructure interior could also be through mesopores. It is in good agreement with the estimated size of the pores in the walls of the tubes/spheres, evidenced in the TEM micrographs. An additional feature observed only in the Ga-NT isotherm, is the presence of a double hysteresis loop, corresponding to the filling of the nanotubes interiors (lower $P/P_0$ values) and the space between the interlaced tubes (higher $P/P_0$ values). Also, the width of the hysteresis loop is broader in the case of Ga-NS. This feature could be the result of more constrained access to the interior of the sphere than in the case of the tubes. From the analysis of the isotherms, it emerged that both structures are characterized by a high specific surface area (500 – 600 $m^2/g$), large pore volume (2 $cm^3/g$) and large mesopores (22 – 27 nm). The textural properties of Ga-NT and Ga-NS were reported in Table 1 and they are in agreement with previous similar solids synthetized by our group.[7, 15]

**Table 1** - Physico-chemical properties of Ga-NT and Ga-NS.

[a] BJH -MPD pore size distribution calculated on the desorption branch of the curve.

[b]t-plots of the two solids reported in figure S10.

| Entry | Solid | $10^{-4}$ mol of Ga / g of catalyst | BET SSA ($m^2/g$) | BJH MPD[a] (nm) | V tot. ($cm^3/g$) | V micro. ($cm^3/g$)[b] |
|---|---|---|---|---|---|---|
| 1 | Ga-NT | 2.2 | 600 | 22 | 2.3 | 0.03 |
| 2 | Ga-NS | 2.1 | 470 | 27 | 2.0 | 0.02 |

The silicon environment of Ga-NT and Ga-NS was characterized *via* $^{29}Si$ Cross Porlarizarion (CP) and Direct Excitation (DE) ss MAS NMR experiments (Figure S11). CP-MAS spectra allowed identifying three different contributions at -110 ppm, -100 ppm and -90 ppm, corresponding respectively to $Q_4$ [$(SiO)_4Si$], $Q_3$ [$(SiO)_3SiOH$] and $Q_2$ [$(SiO)_2Si(OH)_2$] species. To evaluate the proportion of each contribution in the silica matrix quantitative experiments (Figure S11 a and b) were performed as well. In particular, the condensation degree of the silica structure, expressed as

$Q_4/(Q_4+Q_3+Q_2)$ was very similar for nanotubes and nanospheres and was equal to 0.66 and 0.69, respectively. These values agree with previously reported mesoporous silica-based materials, synthesized through a sol-gel method (hydrolytic conditions) and calcined at 550 °C.[56-58] The insertion of gallium in the silica structure is known to induce a combination of Brønsted and Lewis acid sites.[41, 55, 59, 60] The latter are known to activate the acetone molecule, facilitate the attack of glycerol, hence the formation of solketal.[38, 61, 62] Fourier transformed infrared (FT IR) measurements of adsorbed ammonia on Ga-NT and Ga-NS were performed, after outgassing the samples under dynamic vacuum at 400 °C. Figure S13 reported in SI shows the FT IR difference spectra of Ga-NT and Ga-NS upon ammonia dosage (spectrum of the bare outgassed sample has been subtracted). In the low frequency region (1700-1300 $cm^{-1}$) and at high dosage pressure (green and blue curve), the band at 1630 $cm^{-1}$ is attributed to the bending mode of ammonia H-bonded to hydroxyl groups. At lower dosage pressure, the contribution is considerably decreased, and a new band is visible at lower frequency (1620 $cm^{-1}$). The latter can be ascribed to ammonia in interaction with surface Lewis (L) acid sites, due to the presence of unsaturated surface Ga species inserted in the silica framework or extra-framework gallium oxide nanoparticles. The large signal at 1460 $cm^{-1}$ can be associated to the bending mode of $NH_4^+$, because of ammonia protonated from Brønsted (B) acid sites. The presence of this band suggests that the insertion of gallium in the silica framework of nanotubes and hollow nanospheres led to the coordination of silanol -OH moieties with neighboring gallium centers, hence generating Brønsted sites that are acid enough to protonate ammonia.

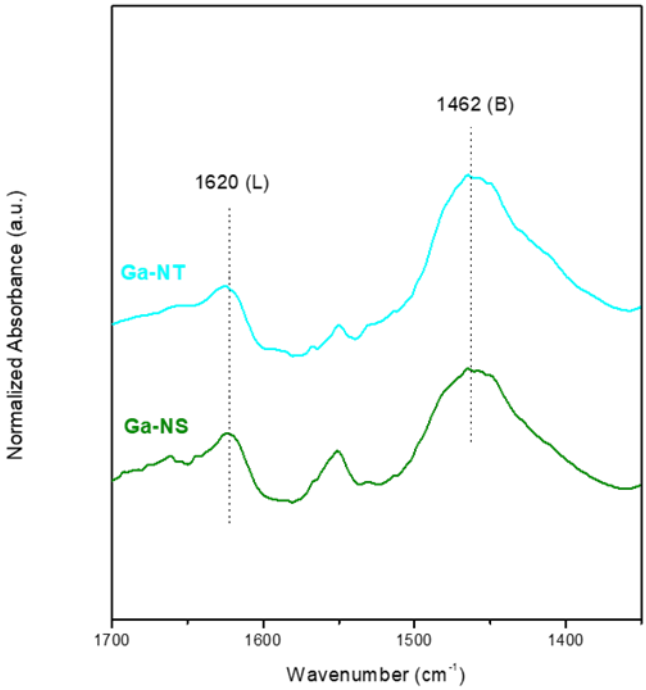


**Figure 5** - Difference FT IR spectra of ammonia dosages on Ga-NT after outgassing at 400 °C (spectrum of the bare outgassed sample has been subtracted). L and B mean Lewis and Brønsted, respectively

Further insights on the acidic properties of Ga-NT and Ga-NS can be deduced by a comparison of their FT-IR spectra registered after the prolongated outgassing of ammonia under dynamic vacuum ($P < 1.10^{-3}$ mbar, *ca.* 30 min). In Figure 5, weak signals due to ammonia molecules interacting with the silica surface are still observable and can be associated to irreversibly formed species. For both Ga-NT and Ga-NS, the bands at 1620 $cm^{-1}$ and 1460 $cm^{-1}$ are still present after prolongated outgassing. The relative intensities and frequencies of the L and B bands are very similar for Ga-NT and Ga-NS, suggesting very similar insertion of gallium species into the silica framework.[41] From this investigation it emerged that the two solids display very similar B and L sites.

To shed more light on the acid properties of the two solids in the optic of highlighting any possible differences arising from the different morphology the analysis via ssNMR was attempted. It is known, that the use of probe molecules such as trimethylphosphine (TMP), trimethylphosphine oxide (TMPO), pyridine (Py), acetonitrile and others analyzed via solid-state NMR technique can provide important information on the nature of the acid sites (L or B) and on their relative strength.[18] Specific contributions are observed via $^{31}P$ solid-state NMR for TMP interacting with Brønsted or Lewis acid sites. TMP interacting with Brønsted sites induces the appearance of signals in the range between -2 and -5 ppm. When the probe-molecule interacts with Lewis sites, contributions in the range -20 to -60 ppm can be observed.[16] It should be mentioned that TMP is an easily oxidable molecule. In the presence of small quantity of oxygen, it oxidizes into TMPO hence a careful control of experimental set-up is needed. Figure S14 also shows the chemical shift ranges of TMPO interacting with both Brønsted and Lewis sites (from 50 to 60 ppm and from 60 to 90 ppm, respectively).[18] It is worth to say that the peaks chemical shift range mentioned for TMPO are still under debating[63] and those reported above are the most commonly used.

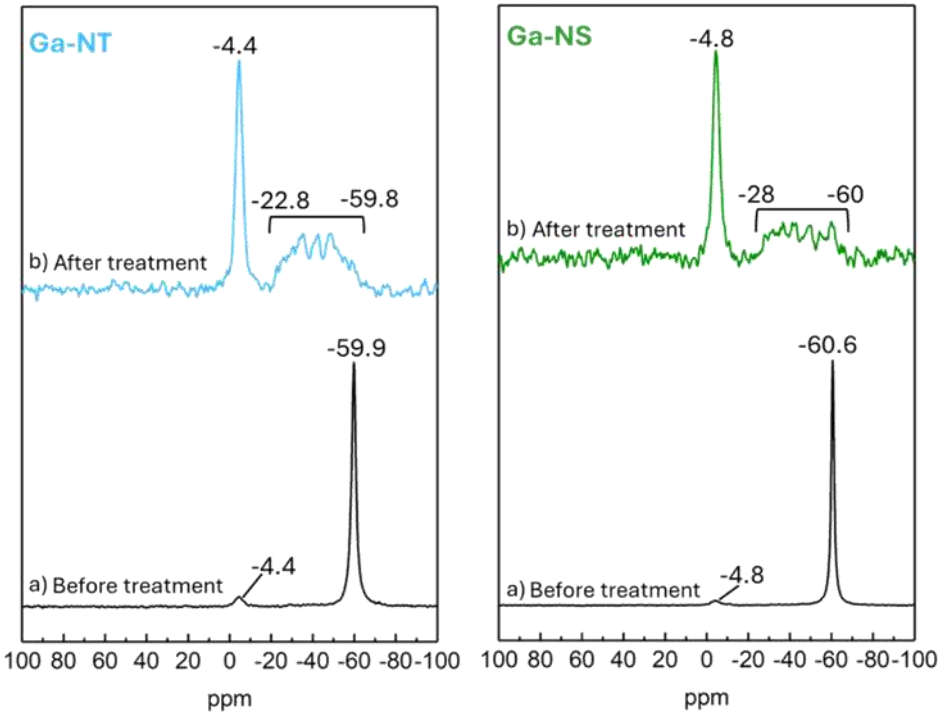



**Figure 6.** $^{31}$P ssNMR spectra of TMP adsorbed on Ga-NT (left) and on Ga-NS (right). a) before and b) after the evacuation treatment.

The results of this analysis are shown in Figure 6 for both NS and NT. After the addition of the probe molecule, the signal of the physisorbed TMP is observed at *ca.* -60 ppm, while the signal of TMP bound to Brønsted active sites is detected at *ca.* -4.5 ppm (before the treatment – black line). The excess of TMP was carefully evacuated under vacuum (*ca.* $8x10^{-3}$ mbar) at 100 °C for 4 h. As expected, after this treatment (Figure 6 dark green and blue curves), the signal of the physiosorbed TMP disappeared. Interestingly, both the intensity and chemical shift of the signal of TMP interacting with Brønsted acid sites were not affected thus indicating that the Brønsted sites are strong enough to preserve the bonded TMP from desorption. Moreover, in the spectral region ranging between -20 and -60 ppm, a broad contribution ascribed to the presence of Lewis acid sites clearly appeared. This result highlights a broad population of Lewis acid sites of different strengths accessible to the TMP probe.[16] A comparison between the obtained spectra of the treatment of Ga-NT and Ga-NS is with TMP reported in Figure S15. The two materials show almost the same signal patterns, with very similar chemical shift values thus indicating a similar strength of acid sites. However, Ga-NT showed a distribution of signals slightly shifted to higher chemical shifts compared to Ga-NS. This result suggests a slightly higher strength of Lewis acid sites for Ga-NT compared to Ga-NS.[9] It is worth noting that in all the spectra there is no peak in the 50 to 90 ppm range (i.e. TMPO), thus indicating

that the set-up employed fully prevents the oxidation of TMP. In light of these analyses, it is possible to assess the B/L ratio by comparing the area of peaks assigned to the TMP bound to Lewis and Brønsted active sites. This evaluation revealed that Ga-NS displays a higher B/L ratio (i.e. 1.03) in comparison with Ga-NT (i.e. 0.75). It is well known that for the target reaction of glycerol conversion, a higher quantity of Brønsted in comparison to the Lewis active sites improves the catalytic performances.[38, 62]

Finally, a series of $^{71}$Ga NMR spectra were recorded to directly probe the chemical environment of gallium species (Figure S16). For the latter NMR analyses, the samples were treated in the same conditions employed for acidity measurements. Interestingly, after calcination and dehydration process under vacuum, no $^{71}$Ga NMR signal was detected (Figure S16a). This observation could be ascribed to a more heterogeneous and/or asymmetric environment of the gallium species. Indeed, the larger quadrupolar coupling constants (CQ) induces a broadening of $^{71}$Ga signals that cannot be longer detectable at least at the concentration of gallium in the nanostructured solids.[45] However, after the addition of 5 µL TMP (Figure S16b), a signal centered at around 144 ppm was observed. This result proves that the coordination of TMP to the Ga atoms induces a decrease of CQ values, allowing the detection of Ga (IV) signals. To obtain conditions more similar to the spectra shown in Figure 2, 20 µL and 40 µL of water were added to the dehydrated solid prior to NMR analysis. From figures S16c and S16d, it is clear that the presence of water also affects the chemical environment of the gallium, most probably increasing its symmetry, thus decreasing the CQ and allowing the $^{71}$Ga signals to be detectable (as previously described for TPM). These observations indicate that the accessible gallium centers are sensitive to the presence of TMP (and water), hence available to the interaction with reactants in solution. To prove this hypothesis, a similar experiment employing acetone as probe molecule was performed as well. Considering that this molecule acts as both solvent and reagent in the reaction under study in this work, it is interesting to evaluate the acetone-Ga interaction. Hence, 40 µL of acetone were used to test the accessibility of this molecule to the Ga active sites. As is possible see in Figure S16e, acetone shows good interaction with Ga, a peak shifted towards 140 ppm appeared; furthermore, the width of the signal indicates a high quadrupolar constant and an asymmetrical gallium environment. Finally, considering the influence of water content within the solids, additional NMR experiments were performed selecting Ga-NS 450 °C, Ga-NS 550 °C, and Ga-NS 650 °C as reference materials. Figure S16 II and S16 III present the $^{71}$Ga ssNMR spectra of dehydrated (S16 II) and hydrated samples (S16 III), the latter obtained by adding 40 µL of water. This additional set of data was added to improve the comparison between the three solids, enhancing the signal-to-noise ratio with respect to the spectra reported in Figure 3. It is worth noting that this

novel set of data confirms the previous claim. Indeed, Figure S16 III shows clearly a progressive increase of extra-framework Ga species as a function of increasing calcination temperature.

**3.3 Study of the catalytic activity of Ga-NS and Ga-NT.** The catalytic activity of the two nanostructures (Ga-NT and Ga-NS) was compared by evaluating the formation of solketal over time (kinetic study, Figure 7). For the sake of comparison, catalytic tests employing pristine silica nanospheres (Si-NS) and nanotubes (Si-NT) were performed as well. These tests showed a very low conversion of glycerol corresponding to a solketal yield lower than 2% (see entries 1 and 2, Table S2). For both NT and NS, the yield of solketal rapidly increased during the first hours of reaction before approaching a plateau at a yield of *ca.* 60 %. A plateau appearing at similar solketal yield was already reported by authors working under similar conditions and was attributed to the thermodynamic equilibrium of the reaction.[39, 61, 64, 65] Moreover, it is interesting to highlight that the yield of solketal increased faster in the case of Ga-NS than for Ga-NT. For example, 2 hours after initial mixing of the reagents, the yield of solketal reached 41 % for nanospheres and 34 % for nanotubes with an associated selectivity of 91 % and 88 %, respectively.

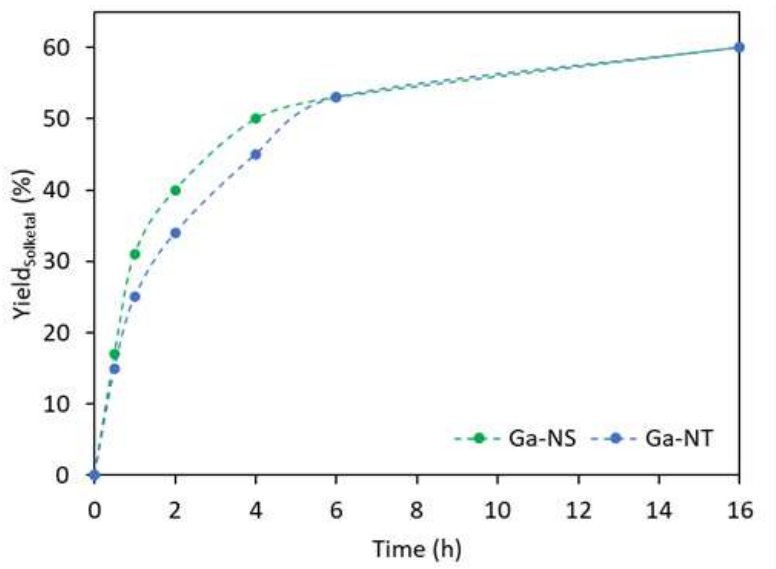



**Figure 7** - kinetic study on Ga-NS and Ga-NT in the conversion of glycerol into solketal. Reaction conditions: 50 °C, 10 mg of catalyst, Gly: Ac = 1 (0.01 mol): 4. Conversion estimated via $^{1}$H NMR of the reaction mixture.

To compare the catalysts in a statistically meaningful way, the yield of solketal was evaluated several times, also considering different batches of catalysts. Moreover, the intrinsic catalytic activity was expressed in the form of a turnover frequency (TOF), evaluated by dividing the number of mole of solketal produced by the experimental amount of gallium calculated from ICP-OES as well as by the

reaction time of 2 h (TOF ($h^{-1}$) = mol solketal/mol Ga x h). The mean TOF value, calculated on a data set composed of minimum 6 values, was equal to 776 $h^{-1}$ and 985 $h^{-1}$ for Ga-NT and Ga-NS, respectively thus indicating that Ga-NS displays better catalytic performances. Considering the very similar physico-chemical properties and coordination environment of Ga species in both Ga-NT and Ga-NS, the enhanced catalytic activity of Ga-NS could be ascribed to the slightly higher B/L acid ratio evidenced via $^{31}P$ ssNMR investigation most probably as a consequence of the more defective structure of NS. Moreover, a more favorable diffusion pathway of the products from the interior of the hollow nanospheres to the exit points could be considered as well to explain the difference of catalytic activity (Figure S17). It deserves to be mentioned that catalytic tests performed at different stirring speeds showed similar yield hence indicating that other parameters such as external diffusion limitation can be neglected.

The heterogeneous nature of the best catalyst (Ga-NS calcined at 550 °C) was further investigated in the conversion of glycerol into solketal. A catalytic test was carried out for one hour after which the catalyst was separated from the reaction mixture and the yield of solketal was evaluated (Figure 8a). The filtrate was then let to react for an additional 5 hours and the yield of solketal was again measured. The yield remained unchanged, indicating that no catalytically active species were leached from the solid to the reaction medium. In addition, figure 8b shows that Ga-NS preserved its excellent selectivity and stable activity for four consecutive catalytic cycles. Between cycles, the catalyst was reactivated thanks to a simple thermal treatment. After the last cycle, Ga-NS was characterized and compared to the fresh Ga-NS. The quantity of gallium evaluated *via* ICP-OES was equal to the one of the fresh solid (2.1 mol/g, compare with entry 2 in Table 1), indicating that the reaction cycles did not alter the Ga content. Moreover, both the morphology and the environment of Ga were very similar to the fresh Ga-NS (Figure S18), suggesting the stability of both the nanosphere structure and the Ga environment, after 4 consecutive catalytic cycles. Hence, Ga-NS show a high potential as heterogeneous catalyst in the conversion of glycerol into solketal.

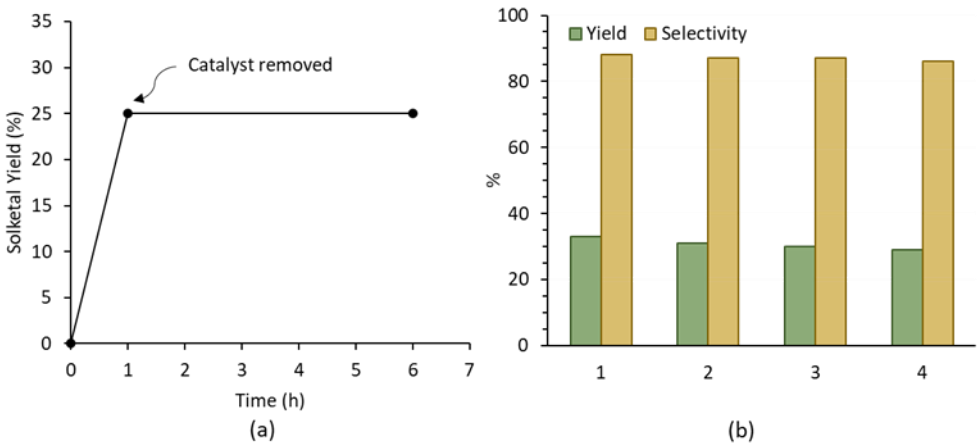


**Figure 8** – Hot filtration test (Ga leaching test). Conditions: 1 h, 50 °C, Gly: Ac = 1: 4, 600 µL EtOH, 10 mg catalyst. The catalyst was removed from the mixture after 1h by centrifugation and let it reacted in the same conditions for 5 supplementary hours. (a) and recycling test. Conditions: 1 h, 50 °C, Gly: Ac = 1: 4 (b) on Ga-NS. Conversion estimated via $^{1}$H NMR of the reaction mixture.

The E-factor, corresponding to the ratio between the mass of waste formed and the mass of desired product obtained, was calculated to measure the sustainability of our catalytic process.[66] The E-factor was evaluated using 30 mg of Ga-NS, 50 °C, Gly: Ac = 1 (0.03 mol): 4 and a time of 16 h (to reach maximum conversion in these conditions). According to the following calculation: [2.76 g glycerol + 6.96 g acetone – 5.77 g acetone recovered by distillation – 2.38 g solketal)/ 2.38 g solketal], the E-factor is equal to 0.66. This low value is in the same range as typical values reported for the industrial production of bulk chemical, supporting the fact that the process is promising.[28]The activity of Ga-NS was compared with catalysts from literature, tested in the same conditions as reported in this manuscript. From the comparison in Figure 9a emerged that Ga-NS outperformed other heterogeneous catalysts previously reported in literature. Note that a particularly interesting comparison of the catalytic performances can be made between Ga-NS and Ga-PNS[55]. Both solids displayed a spherical morphology, similar particle diameter and insertion of tetrahedral gallium (Si/Ga = 74). Compared to Ga-NS, Ga-PNS did not display a hollow interior but instead, a porous network (pore size *ca.* 3 nm). Even if other parameters cannot be excluded, this structural difference could explain the improved performance of Ga-NS compared to Ga-PNS.

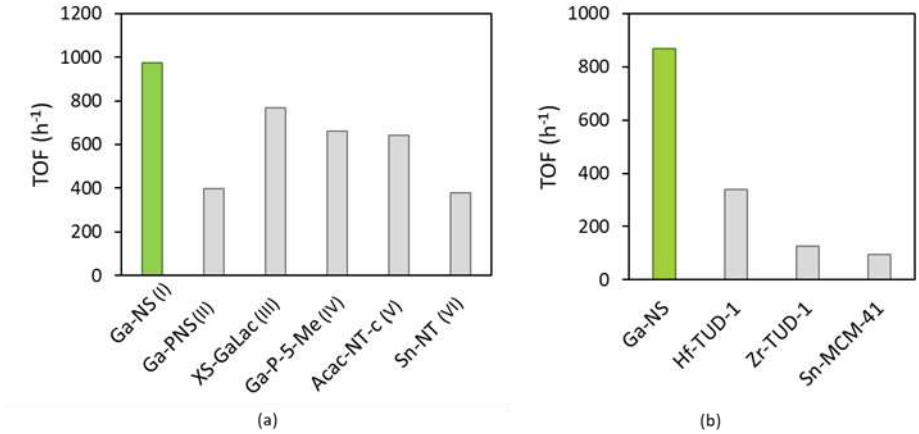



**Figure 9** – Comparison of Ga-NS with catalysts from literature: (a) tested in the following conditions: 50 °C, 10 mg of catalyst, Gly: Ac = 1 (0.01 mol): 4, 2 h. (I)[55], (II)[11], (III)[39], (IV)[15] (V).[67] (VI) 80 °C, 10 mg of catalyst, Gly: Ac = 1 (0.01 mol): 1, 1 h, 1.48 g of tert-butanol. b) The TOF of Hf-TUD-1, Zr-TUD-1 and Sn-MCM-41 were calculated based on data extrapolated from the kinetic.[38]

Comparison with M-doped mesoporous silicates reported in literature and operating in different conditions should be done with care. Note that comparison with catalysts failing the recycling test or evaluation of the activity (TOF) at the thermodynamic plateau, are not considered herein.[68-72] However, a relevant comparison can be done with Hf-TUD-1, Zr-TUD-1 and Sn-MCM-41 (Figure 9b).[38] The authors performed the conversion of glycerol into solketal using t-butanol as solvent, a 1 (0.01 mol): 1 molar ratio of glycerol to acetone, 25 mg of catalyst and a temperature of 80 °C. To further investigate the behavior of our catalyst in these synthesis conditions, the yield of solketal was measured at different times. After 2 h, the yield of solketal was equal to 25 % (entry 1 in Table 3). Decreasing the reaction time to 1 h and 0.5 h did not result in any decrease of solketal produced (Table 3, entries 2 and 3). This result indicates that a plateau is already reached after 0.5 hours of reaction. To better approach the intrinsic activity of Ga-NS, the catalyst mass was decreased. Reducing the quantity of catalyst to 10 mg (instead of 25 mg), an evolution of solketal yield with time was observed and 25 % of yield was reached after 24 h of reaction (Table 3, entries 4 and 5). To investigate if a yield of 25 % was associated with the thermodynamic plateau, an additional catalytic test was performed adding 10 mg of fresh catalyst 24 hours after the beginning of the reaction (Table3, entry 8). The yield of solketal was then measured after one additional hour of reaction and remained equal to 24 %. From the comparison between entries 6 and 7 in Table 3, it emerged that the thermodynamic equilibrium was achieved around 25 % in yield. Note that adapting the reaction conditions (Table 3, entry 8) allowed us to considerably increase the yield of solketal to 87 %, being close to the total conversion of glycerol. Hence, the conditions reported in Table 3 in entries 4 and 5 allowed approaching the initial activity of Ga-NS, far from thermodynamic equilibrium, when working with a 1: 1 molar ratio of glycerol to acetone, a temperature of 80 °C and t-butanol as solvent. In these conditions, a TOF can be approached and reaches 1142 $h^{-1}$ (calculated from entry 4 in Table 3). The comparison between materials presents in literature and bearing different metals is presented in Figure 9b. From this comparison emerged that Ga-NS outperformed the other catalysts. This improved catalytic performance probably arises from a series of favorable features such as the advantageous silica nanostructure, nature of the heteroelement and appropriate environment of the Ga centers resulting in a high B/L acid ratio.

**Table 3**– Conversion of glycerol into solketal with Ga-NS considering Gly (0.01 mol): Ac = 1: 1, 80 °C, 1.48 g of tert-butanol. *Conditions of entry 7: 10 mg of fresh catalyst added after 24 h of reaction **Condition of entry 8: Gly (0.01 mol): Ac = 1: 15, 50 °C. Conversion estimated via $^{1}$H NMR of the reaction mixture.

| Entry | m catalyst (mg) | Time (h) | Yield (%) | Selectivity (%) |
|---|---|---|---|---|
| 1 | 25 | 2 | 25 | 97 |
| 2 | 25 | 1 | 26 | 97 |
| 3 | 25 | 0.5 | 26 | 97 |
| 4 | 10 | 0.5 | 12 | 93 |
| 5 | 10 | 1 | 17 | 100 |
| 6 | 10 | 24 | 25 | 100 |
| 7* | 10 + 10 | 24 + 1 | 24 | 100 |
| 8** | 20 | 16 | 87 | 98 |

## 4. CONCLUSION

Two Ga-doped silica materials namely Ga-NT and Ga-NS, were synthesized through a soft-templated sol-gel approach. The morphology of the Ga-$SiO_2$ nanostructures was accurately controlled, through the variation of the stirring speed. Both Ga-doped nanotubes and hollow nanospheres displayed Ga centers with similar coordination environment that was controlled through the simple variation of the calcination temperature. Solid state $^{71}$Ga MAS NMR suggested that the increase of the temperature led to a rearrangement of the active phase consisting to the surface migration and increase of Ga coordination number. A temperature of 550 °C was found to be the best compromise to enhance the production of solketal. Both solids displayed similar textural and acidic properties. FT-IR measurements using ammonia and $^{31}$P ssNMR with TMP as probe molecules evidenced a minor difference in terms of Lewis acidic strength and different B/L ratio. The two synthesized catalysts were tested for the conversion of glycerol to solketal. Both solids showed promising activities. However, the kinetic study clearly evidenced that Ga-NS favors the faster formation of the targeted product (i.e. solketal). This result was attributed to higher amount of Brønsted active sites, the slight weakness of the Lewis active sites and probably to the morphology of the solid reducing diffusion limitations. Furthermore, Ga-doped silica nanospheres were reused in multiple cycles thus providing the stability of the material under selected reaction conditions. Finally, Ga-NS were compared with different solids reported in literature showing an outstanding catalytic activity with TOF values above 800 $h^{-1}$.

## ASSOCIATED CONTENT

**Supporting Information**. Experimental procedures, $^{29}$Si and $^{71}$Ga ssNMR experiments, TEM images, X-Ray analysis, $N_2$-physisorption, FT-IR spectra, $^{31}$P ssNMR analysis, schematic representation of diffusion process in Ga-NT and Ga-NS.

## AUTHOR INFORMATION


### Corresponding Author

* **Carmela Aprile** - Unit of Nanomaterials Chemistry, Department of Chemistry, NISM, University of Namur,5000 Namur, Belgium. Email: Carmela.Aprile@unamur.be

*__Luca Fusaro__ - Unit of Nanomaterials Chemistry, Department of Chemistry, NISM, University of Namur,5000 Namur, Belgium. Email: Luca.Fusaro@unamur.be

### Authors

**Loraine Soumoy** - Unit of Nanomaterials Chemistry, Department of Chemistry, NISM, University of Namur,5000 Namur, Belgium. Email: Loraine.soumoy@unamur.be

**Anthony Morena** – Unit of Nanomaterials Chemistry, Department of Chemistry, NISM, University of Namur,5000 Namur, Belgium. Email: Anthony.Morena@unamur.be

**Damien P. Debecker** - *Université catholique de Louvain (UCLouvain), Institute of Condensed Matter and Nanosciences (IMCN), 1348 Louvain-la-Neuve, Belgium*. Email: Damien.debecker@uclouvain.be

**Marco Armandi** - Department of Applied Science and Technology, Politecnico di Torino, 10129 Torino, Italy. Email: marco.armandi@polito.it

**Sonia Fiorilli** - Department of Applied Science and Technology, Politecnico di Torino, 10129 Torino, Italy. Email: sonia.fiorilli@polito.it


### Author Contributions

L.S. and A.M Methodology, investigation, data curation, writing- original draft preparation. S.F., M.A. and D.P.D. review editing and validation. C.A. and L.F. supervision, funding acquisition, methodology, writing- original draft preparation, validation. The manuscript was written through contributions of all authors. ‡These authors contributed equally.


### Funding Sources

Ph.D. Grant FNRS – G4/1/6-GEQ/CDB

PdR project – T.0004.21

EOS project – 0.0032.22


### Notes

The authors declare no competing financial interest.

## ACKNOWLEDGMENT

The authors acknowledge the FNRS for the financial support including via the research project grant G4/1/6-GEQ/CDB, the PdR project T.0004.21 and EOS project 0.0032.22. L.S. thanks the FNRS for the financial support in the context of her FRIA PhD grant. This research used resources of PC2(Plateforme Technologique Physico-Chemical Characteriza-tion) and MORPH-IM (Morphology & Imaging) technologyplatforms located at the University of Namur.

## REFERENCES

[1] L. Beaton, S. Zhang, M. Kruk, Formation of Double-Helical Structures by Silica Nanotubes Templated by Mixtures of Common Nonionic Surfactants in Aqueous Solutions, ACS Nano, 15 (2021) 1016-1029.
[2] L. Huang, M. Kruk, Synthesis of ultra-large-pore FDU-12 silica using ethylbenzene as micelle expander, Journal of Colloid and Interface Science, 365 (2012) 137-142.
[3] L. Soumoy, A. Maertens, A. Morena, L. Fusaro, M. Armandi, S. Fiorilli, D.P. Debecker, C. Aprile, Low dimensional Zr-based catalysts for the effective upgrading of ethyl levulinate to γ-valerolactone, Materials Today Chemistry, 40 (2024) 102189.
[4] A. Comès, J. Theissen, S. Dallemagne, A. Morena, C. Aprile, Imidazolium-Containing Hybrid Organic–Inorganic Materials for the Conversion of CO2: Unveiling the Key Role of the Ionic Template, Inorganic Chemistry, 62 (2023) 21003-21013.
[5] Y. Li, M. Kruk, Single-micelle-templated synthesis of hollow silica nanospheres with tunable pore structures, RSC Advances, 5 (2015) 69870-69877.
[6] N. Pal, J.-H. Lee, E.-B. Cho, Recent Trends in Morphology-Controlled Synthesis and Application of Mesoporous Silica Nanoparticles, Nanomaterials, 10 (2020) 2122.
[7] L. Soumoy, L. Fusaro, D.P. Debecker, C. Aprile, Low-Dimensional Hollow Nanostructures: From Morphology Control to the Release of an Active Pharmaceutical Ingredient, Chemistry of Materials, 35 (2023) 1877-1890.
[8] E.M. Flanigen, Chapter 2 Zeolites and Molecular Sieves an Historical Perspective, in: H. van Bekkum, E.M. Flanigen, J.C. Jansen (Eds.) Studies in Surface Science and Catalysis, Elsevier1991, pp. 13-34.
[9] G. Yang, L. Zhou, X. Han, Lewis and Brönsted acidic sites in M4+-doped zeolites (M=Ti, Zr, Ge, Sn, Pb) as well as interactions with probe molecules: A DFT study, Journal of Molecular Catalysis A: Chemical, 363-364 (2012) 371-379.
[10] M. Shamzhy, M. Opanasenko, P. Concepción, A. Martínez, New trends in tailoring active sites in zeolite-based catalysts, Chemical Society Reviews, 48 (2019) 1095-1149.
[11] H. Hussein, A. Vivian, L. Fusaro, M. Devillers, C. Aprile, Synthesis of Highly Accessible Gallosilicates via Impregnation Procedure: Enhanced Catalytic Performances in the Conversion of Glycerol into Solketal, ChemCatChem, 12 (2020) 5966-5976.
[12] E. Peeters, G. Pomalaza, I. Khalil, A. Detaille, D.P. Debecker, A.P. Douvalis, M. Dusselier, B.F. Sels, Highly Dispersed Sn-beta Zeolites as Active Catalysts for Baeyer–Villiger Oxidation: The Role of Mobile, In Situ Sn(II)O Species in Solid-State Stannation, ACS Catalysis, 11 (2021) 5984-5998.
[13] I. Istadi, T. Riyanto, L. Buchori, D.D. Anggoro, G. Gilbert, K.A. Meiranti, E. Khofiyanida, Enhancing Brønsted and Lewis Acid Sites of the Utilized Spent RFCC Catalyst Waste for the Continuous Cracking Process of Palm Oil to Biofuels, Industrial & Engineering Chemistry Research, 59 (2020) 9459-9468.
[14] A. Tuel, Modification of mesoporous silicas by incorporation of heteroelements in the framework, Microporous and Mesoporous Materials, 27 (1999) 151-169.
[15] L. Soumoy, C. Célis, D.P. Debecker, M. Armandi, S. Fiorilli, C. Aprile, Hafnium-doped silica nanotubes for the upgrading of glycerol into solketal: Enhanced performances and in-depth structure-activity correlation, Journal of Catalysis, 411 (2022) 41-53.
[16] A. Zheng, S.-B. Liu, F. Deng, 31P NMR Chemical Shifts of Phosphorus Probes as Reliable and Practical Acidity Scales for Solid and Liquid Catalysts, Chemical Reviews, 117 (2017) 12475-12531.
[17] X. Yi, Y.-K. Peng, W. Chen, Z. Liu, A. Zheng, Surface Fingerprinting of Faceted Metal Oxides and Porous Zeolite Catalysts by Probe-Assisted Solid-State NMR Approaches, Accounts of Chemical Research, 54 (2021) 2421-2433.

[18] X. Yi, H.-H. Ko, F. Deng, S.-B. Liu, A. Zheng, Solid-state 31P NMR mapping of active centers and relevant spatial correlations in solid acid catalysts, Nature Protocols, 15 (2020) 3527-3555.
[19] X. Collard, L. Li, W. Lueangchaichaweng, A. Bertrand, C. Aprile, P.P. Pescarmona, Ga-MCM-41 nanoparticles: Synthesis and application of versatile heterogeneous catalysts, Catalysis Today, 235 (2014) 184-192.
[20] P.Y. Dapsens, B.T. Kusema, C. Mondelli, J. Pérez-Ramírez, Gallium-modified zeolites for the selective conversion of bio-based dihydroxyacetone into C1–C4 alkyl lactates, Journal of Molecular Catalysis A: Chemical, 388-389 (2014) 141-147.
[21] Z. Pirzadi, F. Meshkani, From glycerol production to its value-added uses: A critical review, Fuel, 329 (2022) 125044.
[22] H. Xu, H. Li, Alcohol-assisted hydrodeoxygenation as a sustainable and cost-effective pathway for biomass derivatives upgrading, Journal of Energy Chemistry, 73 (2022) 133-159.
[23] P.T. Anastas, J.C. Warner, Principles of green chemistry, Green chemistry: Theory and practice, 29 (1998) 14821-14842.
[24] S. Ao, S.L. Rokhum, Recent Advances in the Valorization of Biodiesel By-Product Glycerol to Solketal, Journal of Chemistry, 2022 (2022) 4938672.
[25] A. Behr, J. Eilting, K. Irawadi, J. Leschinski, F. Lindner, Improved utilisation of renewable resources: New important derivatives of glycerol, Green Chemistry, 10 (2008) 13-30.
[26] J.I. García, H. García-Marín, E. Pires, Glycerol based solvents: synthesis, properties and applications, Green Chemistry, 16 (2014) 1007-1033.
[27] M.R. Nanda, Y. Zhang, Z. Yuan, W. Qin, H.S. Ghaziaskar, C. Xu, Catalytic conversion of glycerol for sustainable production of solketal as a fuel additive: A review, Renewable and Sustainable Energy Reviews, 56 (2016) 1022-1031.
[28] A. Cornejo, I. Barrio, M. Campoy, J. Lázaro, B. Navarrete, Oxygenated fuel additives from glycerol valorization. Main production pathways and effects on fuel properties and engine performance: A critical review, Renewable and Sustainable Energy Reviews, 79 (2017) 1400-1413.
[29] R.A. Sheldon, Metrics of Green Chemistry and Sustainability: Past, Present, and Future, ACS Sustainable Chemistry & Engineering, 6 (2018) 32-48.
[30] G. Zhang, L. Zhang, X. Wang, A. Chen, Q. Zhang, Microfluidic processing of HZSM-5 films in a capillary microreactor for the continuous acetalisation reaction of glycerol with acetone, Reaction Chemistry & Engineering, 5 (2020) 539-546.
[31] R. Gérardy, D.P. Debecker, J. Estager, P. Luis, J.-C.M. Monbaliu, Continuous Flow Upgrading of Selected C2–C6 Platform Chemicals Derived from Biomass, Chemical Reviews, 120 (2020) 7219-7347.
[32] T.N. Pham, T. Sooknoi, S.P. Crossley, D.E. Resasco, Ketonization of Carboxylic Acids: Mechanisms, Catalysts, and Implications for Biomass Conversion, ACS Catalysis, 3 (2013) 2456-2473.
[33] F.D.L. Menezes, M.D.O. Guimaraes, M.J. da Silva, Highly Selective SnCl2-Catalyzed Solketal Synthesis at Room Temperature, Industrial & Engineering Chemistry Research, 52 (2013) 16709-16713.
[34] L. Roldán, R. Mallada, J.M. Fraile, J.A. Mayoral, M. Menéndez, Glycerol upgrading by ketalization in a zeolite membrane reactor, Asia-Pacific Journal of Chemical Engineering, 4 (2009) 279-284.
[35] G. Dizoğlu, E. Sert, Fuel additive synthesis by acetylation of glycerol using activated carbon/UiO-66 composite materials, Fuel, 281 (2020) 118584.
[36] G. Vicente, J.A. Melero, G. Morales, M. Paniagua, E. Martín, Acetalisation of bio-glycerol with acetone to produce solketal over sulfonic mesostructured silicas, Green Chemistry, 12 (2010) 899-907.
[37] J. Kowalska-Kus, A. Held, M. Frankowski, K. Nowinska, Solketal formation from glycerol and acetone over hierarchical zeolites of different structure as catalysts, Journal of Molecular Catalysis A: Chemical, 426 (2017) 205-212.
[38] L. Li, T.I. Korányi, B.F. Sels, P.P. Pescarmona, Highly-efficient conversion of glycerol to solketal over heterogeneous Lewis acid catalysts, Green Chemistry, 14 (2012) 1611-1619.
[39] A. Vivian, L. Soumoy, L. Fusaro, S. Fiorilli, D.P. Debecker, C. Aprile, Surface-functionalized mesoporous gallosilicate catalysts for the efficient and sustainable upgrading of glycerol to solketal, Green Chemistry, 23 (2021) 354-366.
[40] E. Gianotti, M.E. Raimondi, L. Marchese, G. Martra, T. Maschmeyer, J.M. Seddon, S. Coluccia, A Spectroscopic Study of Group IV Transition-Metal-Incorporated Direct Templated Mesoporous Catalysts. Part 2. A Comparison of Ti-, Zr- and Hf-Containing Materials, Catalysis Letters, 76 (2001) 21-26.

[41] A. Vivian, L. Soumoy, L. Fusaro, P. Louette, A. Felten, S. Fiorilli, D.P. Debecker, C. Aprile, The high activity of mesoporous Ga-SiO2 catalysts in the upgrading of glycerol to solketal explained by in-depth characterization, Journal of Catalysis, 400 (2021) 83-92.
[42] A.A. Smirnov, S.A. Selishcheva, V.A. Yakovlev, Acetalization Catalysts for Synthesis of Valuable Oxygenated Fuel Additives from Glycerol, Catalysts, 8 (2018) 595.
[43] A.A.F.d. Costa, A.d.N. de Oliveira, R. Esposito, C. Len, R. Luque, R.C.R. Noronha, G.N.d. Rocha Filho, L.A.S.d. Nascimento, Glycerol and Catalysis by Waste/Low-Cost Materials—A Review, Catalysts, 12 (2022) 570.
[44] A. Styskalik, I. Kordoghli, C. Poleunis, A. Delcorte, C. Aprile, L. Fusaro, D.P. Debecker, Highly porous hybrid metallosilicate materials prepared by non-hydrolytic sol-gel: Hydrothermal stability and catalytic properties in ethanol dehydration, Microporous and Mesoporous Materials, 297 (2020) 110028.
[45] S.R. Docherty, L.A. Völker, A.V. Yakimov, R. Verel, C. Copéret, 71Ga NMR Signatures of Lewis and Brønsted Acid Sites in Gallium Silicates Evidenced and Deciphered upon Interaction with Probe Molecules, The Journal of Physical Chemistry C, 127 (2023) 24552-24563.
[46] M. Hunger, W. Wang, Characterization of Solid Catalysts in the Functioning State by Nuclear Magnetic Resonance Spectroscopy, in: B.C. Gates, H. Knzinger (Eds.) Advances in Catalysis, Academic Press2006, pp. 149-225.
[47] C.R. Bayense, A.P. Kentgens, J.W. De Haan, L.J. Van de Ven, J.H. Van Hooff, Determination of gallium in H (Ga) ZSM5 zeolites by gallium-71 MAS NMR spectroscopy, The Journal of Physical Chemistry, 96 (1992) 775-782.
[48] M. Chatterjee, T. Iwasaki, Y. Onodera, T. Nagase, H. Hayashi, T. Ebina, Characterization of ordered mesoporous gallium MCM-41 synthesized at room temperature, Chemistry of materials, 12 (2000) 1654-1659.
[49] H.K.C. Timken, E. Oldfield, Solid-state gallium-69 and gallium-71 nuclear magnetic resonance spectroscopic studies of gallium analog zeolites and related systems, Journal of the American Chemical Society, 109 (1987) 7669-7673.
[50] S. Wintzheimer, L. Luthardt, K.L.A. Cao, I. Imaz, D. Maspoch, T. Ogi, A. Bück, D.P. Debecker, M. Faustini, K. Mandel, Multifunctional, Hybrid Materials Design via Spray-Drying: Much more than Just Drying, Advanced Materials, 35 (2023) 2306648.
[51] C.O. Areán, M.R. Delgado, V. Montouillout, D. Massiot, Synthesis and Characterization of Spinel-Type Gallia-Alumina Solid Solutions, Zeitschrift für anorganische und allgemeine Chemie, 631 (2005) 2121-2126.
[52] A. Vivian, L. Fusaro, D.P. Debecker, C. Aprile, Mesoporous Methyl-Functionalized Sn-Silicates Generated by the Aerosol Process for the Sustainable Production of Ethyl Lactate, ACS Sustainable Chemistry & Engineering, 6 (2018) 14095-14103.
[53] Z. Wang, Y. Jiang, A. Baiker, J. Huang, Pentacoordinated Aluminum Species: New Frontier for Tailoring Acidity-Enhanced Silica–Alumina Catalysts, Accounts of Chemical Research, 53 (2020) 2648-2658.
[54] Z. Wang, T. Li, Y. Jiang, O. Lafon, Z. Liu, J. Trébosc, A. Baiker, J.-P. Amoureux, J. Huang, Acidity enhancement through synergy of penta- and tetra-coordinated aluminum species in amorphous silica networks, Nature Communications, 11 (2020) 225.
[55] A. Maertens, A. Vivian, L. Fusaro, A. Felten, P. Louette, M. Armandi, S. Fiorilli, C. Aprile, Low-impact synthesis of mesostructured acidic catalysts: toward the efficient conversion of crude glycerol, Sustainable Energy & Fuels, 6 (2022) 3818-3829.
[56] M. Luhmer, J.B. d'Espinose, H. Hommel, A.P. Legrand, High-resolution 29Si solid-state NMR study of silicon functionality distribution on the surface of silicas, Magnetic Resonance Imaging, 14 (1996) 911-913.
[57] A. Steel, S.W. Carr, M.W. Anderson, 29Si solid-state NMR study of mesoporous M41S materials, Chemistry of materials, 7 (1995) 1829-1832.
[58] R. Ojeda-López, I.J. Pérez-Hermosillo, J. Marcos Esparza-Schulz, A. Cervantes-Uribe, A. Domínguez-Ortiz, SBA-15 materials: calcination temperature influence on textural properties and total silanol ratio, Adsorption, 21 (2015) 659-669.
[59] Y. Zhou, H. Thirumalai, S.K. Smith, K.H. Whitmire, J. Liu, A.I. Frenkel, L.C. Grabow, J.D. Rimer, Ethylene Dehydroaromatization over Ga-ZSM-5 Catalysts: Nature and Role of Gallium Speciation, Angewandte Chemie International Edition, 59 (2020) 19592-19601.
[60] E.A. Uslamin, B. Luna-Murillo, N. Kosinov, P.C.A. Bruijnincx, E.A. Pidko, B.M. Weckhuysen, E.J.M. Hensen, Gallium-promoted HZSM-5 zeolites as efficient catalysts for the aromatization of biomass-derived furans, Chemical Engineering Science, 198 (2019) 305-316.

[61] M.R. Nanda, Z. Yuan, W. Qin, H.S. Ghaziaskar, M.-A. Poirier, C.C. Xu, Thermodynamic and kinetic studies of a catalytic process to convert glycerol into solketal as an oxygenated fuel additive, Fuel, 117 (2014) 470-477.
[62] K. Stawicka, A.E. Díaz-Álvarez, V. Calvino-Casilda, M. Trejda, M.A. Bañares, M. Ziolek, The Role of Brønsted and Lewis Acid Sites in Acetalization of Glycerol over Modified Mesoporous Cellular Foams, The Journal of Physical Chemistry C, 120 (2016) 16699-16711.
[63] C. Bornes, M. Fischer, J.A. Amelse, C.F.G.C. Geraldes, J. Rocha, L. Mafra, What Is Being Measured with P-Bearing NMR Probe Molecules Adsorbed on Zeolites?, Journal of the American Chemical Society, 143 (2021) 13616-13623.
[64] M.N. Moreira, R.P.V. Faria, A.M. Ribeiro, A.E. Rodrigues, Solketal Production from Glycerol Ketalization with Acetone: Catalyst Selection and Thermodynamic and Kinetic Reaction Study, Industrial & Engineering Chemistry Research, 58 (2019) 17746-17759.
[65] F. Taddeo, R. Esposito, V. Russo, M. Di Serio, Kinetic Modeling of Solketal Synthesis from Glycerol and Acetone Catalyzed by an Iron(III) Complex, Catalysts, 11 (2021) 83.
[66] D.P. Debecker, K. Kuok Hii, A. Moores, L.M. Rossi, B. Sels, D.T. Allen, B. Subramaniam, Shaping Effective Practices for Incorporating Sustainability Assessment in Manuscripts Submitted to ACS Sustainable Chemistry & Engineering: Catalysis and Catalytic Processes, ACS Sustainable Chemistry & Engineering, 9 (2021) 4936-4940.
[67] L.A. Bivona, A. Vivian, L. Fusaro, S. Fiorilli, C. Aprile, Design and catalytic applications of 1D tubular nanostructures: Improving efficiency in glycerol conversion, Applied Catalysis B: Environmental, 247 (2019) 182-190.
[68] Z. Li, Z. Miao, X. Wang, J. Zhao, J. Zhou, W. Si, S. Zhuo, One-pot synthesis of ZrMo-KIT-6 solid acid catalyst for solvent-free conversion of glycerol to solketal, Fuel, 233 (2018) 377-387.
[69] S. Ammaji, G.S. Rao, K.V.R. Chary, Acetalization of glycerol with acetone over various metal-modified SBA-15 catalysts, Applied Petrochemical Research, 8 (2018) 107-118.
[70] Y. Huang, G. Zhang, Q. Zhang, Preparation of the WOX/MCM-41 Solid Acid Catalyst and the Catalytic Performance for Solketal Synthesis, ACS Omega, 6 (2021) 3875-3883.
[71] T.H. Abreu, C.I. Meyer, C. Padró, L. Martins, Acidic V-MCM-41 catalysts for the liquid-phase ketalization of glycerol with acetone, Microporous and Mesoporous Materials, 273 (2019) 219-225.
[72] N. Chansorn, S. Amnuaypanich, S. Soontaranon, S. Rugmai, S. Amnuaypanich, Increasing solketal production from the solventless ketalization of glycerol catalyzed by nanodispersed phosphotungstic acid in poly(N-methyl-4-vinylpyridinium) grafted on silica nanoparticles, Journal of Industrial and Engineering Chemistry, 112 (2022) 233-243.